ACS ES&T Water

pubs.acs.org/estwater

Article

Salinity Stress Modulates the Dynamic Co-occurrence Interactions between DOM and Microbial Community Profiles in a Typical River−Estuary−Ocean Continuum: From the Pearl River to South China Sea

Chao Zhang,[#] Yingqiang Li,[#] Junyu Zhu,[#] Zhe Zhang, Yue Xie, Shuna Fu, Wanbing Zheng, Zihan Shen, Bangxing Ren, Zhenguo Chen, Haijun He,* Guang-Guo Ying, Harald Horn, Amy M. McKenna, and Mingzhi Huang*

Cite This: *ACS EST Water* 2025, 5, 2096−2109

Read Online

ACCESS | Metrics & More | Article Recommendations | Supporting Information

ABSTRACT: The pivotal role of salinity stress in regulating the microbial-driven dissolved organic matter (DOM) transformation in river−estuary−ocean continua has consistently been overlooked. The difference in the osmotic pressure caused by the salinity fluctuations between freshwater and seawater results in the formation of distinct microbial community profiles, subsequently triggering dynamic DOM transformation. However, the complexity of the dynamic interactions poses a vital challenge in unraveling the underlying mechanisms at the molecular level. To bridge this gap, the utilization of FT-ICR MS, integrated with co-occurrence network, emerges as a potent tool. In this study, we demonstrated that, despite the major influence of urbanization on the DOM input, as characterized by spectroscopic characteristics, its impact on the transformation processes of DOM is negligible when compared to the salinity stress. In contrast, salinity can trigger similar transformation patterns of DOM among diverse microbial populations, underscoring the pivotal role of salinity. Concurrently, salinity enhances microbial transformations of DOM (e.g., higher biological index and the ratio of product to precursor), and furthermore, the gradual increase in total nitrogen with increasing salinity may be correlated with the salinity-induced suppression of denitrifying bacteria. The co-occurrence network analysis offers mechanistic insights into delineating the intricate interplay of synergism and antagonism among microbial DOM transformations under salinity conditions.

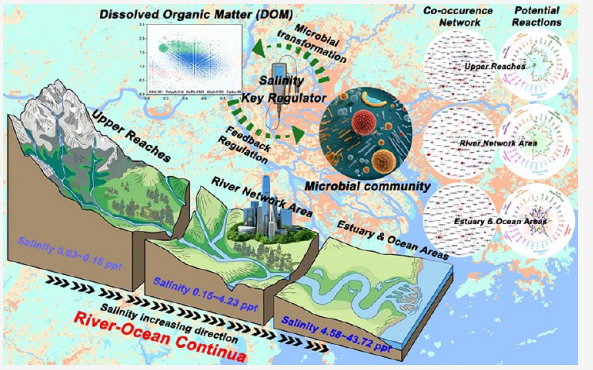

KEYWORDS: *dissolved organic matter, FT−ICR MS, co-occurrence network analysis, salinity stress, river−ocean continua*

1. INTRODUCTION

River−ocean continua play vital roles in connecting terrestrial and marine ecosystems, facilitating the transportation and transformation of dissolved organic matter (DOM), originating from each side.[1,2] An estimated 0.25 Pg C yr^{-1} of DOM is transferred through rivers to oceans globally.[3] Simultaneously, oceans receive approximately 2.0 Pg C yr^{-1} of DOM inputs originating from the decomposition and excretion processes within marine ecosystems.[4] DOM in river−ocean continua, as one of the largest reservoirs of exchangeable organic carbon on the planet Earth, results from partial decomposition and transformation of the material input by microbes.[5] This process, involving the storage and turnover of DOM, is intricate and dynamic, influenced by water environment conditions (e.g., salinity) and the amount of input materials.[6] In turn, the dynamics impact productivity and development of river−ocean continua.[7] The long-term balance between material inputs and microbial decomposition determines the quantity and composition of DOM.[8] Recent studies have highlighted the vital significance of microbial community fingerprints in shaping DOM formation and its persistence.[9,10] Specifically, these microbes govern the carbon cycle predominantly through two important roles: catabolism-mediated carbon decomposition and anabolism-induced carbon stabilization.[9] Meanwhile, the chemical properties of DOM influence the structure and functioning of microbial communities in the river−ocean continua, as DOM represents their primary

Received: September 2, 2024
Revised: March 22, 2025
Accepted: March 31, 2025
Published: April 7, 2025

https://doi.org/10.1021/acsestwater.4c00832
ACS EST Water 2025, 5, 2096−2109

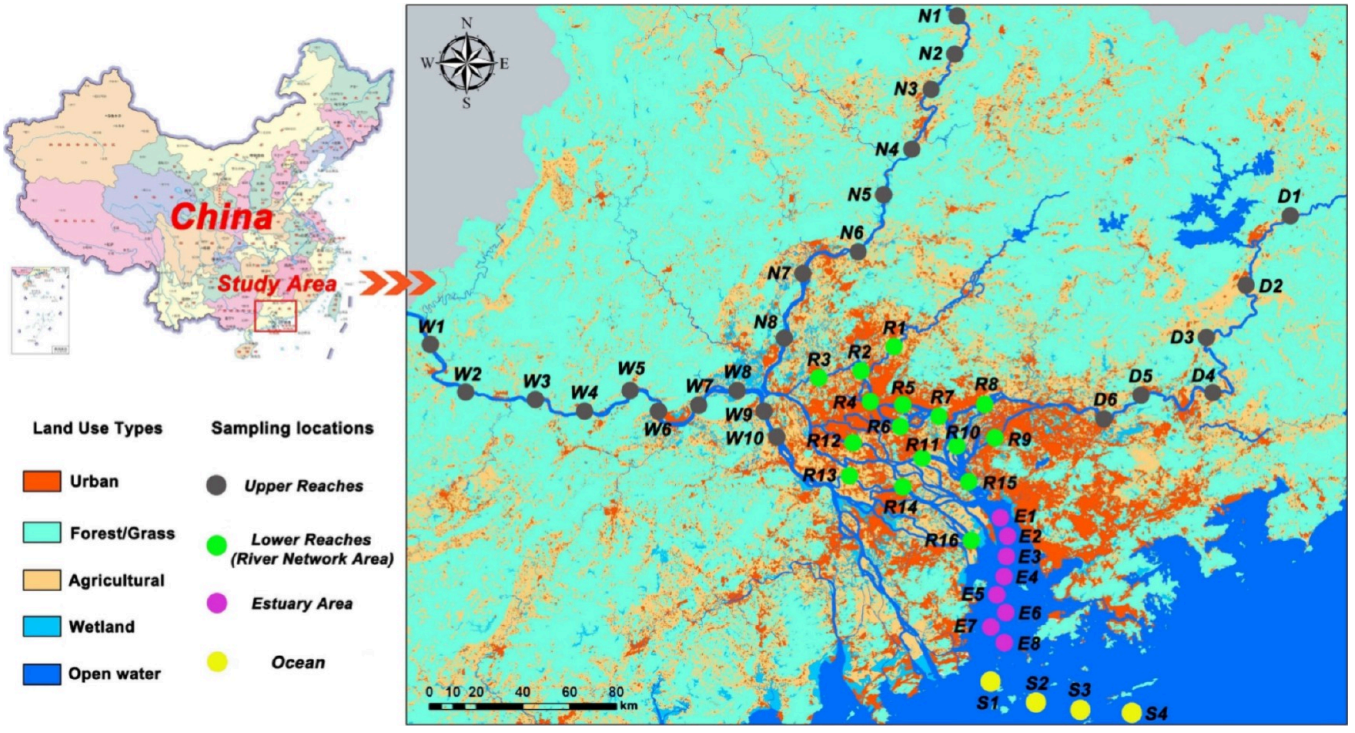

Figure 1. Map of study area and sampling sites from the Upper Reaches of the Pearl River to the Ocean (South China Sea).

energy source.[11] Consequently, understanding the complex interconnections between microbial communities and DOM is vital to elucidating the carbon cycle in the river−ocean continua. However, the diversity of microbial communities and the complexity of DOM chemistry pose substantial challenges to fully grasping this intricate relationship.[12] In conjunction with tidal current interaction in the river−ocean continua, different sections (i.e., the upper reach, the lower reach, the estuary, and the ocean) preserve distinctive molecular signatures of DOM and its potential transformation patterns as well.[13−15]

The remarkable cellular osmotic pressure disparities induced by salinity prevent marine microbes from surviving in freshwater environments (conversely, freshwater microbes struggle in marine high-salinity environments), giving rise to uniquely tailored microbial communities in both river and ocean ecosystems.[12,16] When combined with tidal current interaction, salinity-gradient variation and the consequent differences in microbial communities generally form along river courses, extending from the upper reaches to the ocean.[17,18] However, the impact of the microbial community difference on the bioavailability and transformation of DOM along the salinity gradient is rarely studied, especially at the molecular level. It warrants further exploration to elucidate complex relationships between aquatic microbial communities and DOM along the salinity gradient, aiming to enhance our understanding of the carbon cycle in the river−ocean continua. The Pearl River, the largest river system that merges into the South China Sea, nurtures one of the largest bay areas on a global scale.[19,20] It comprises three major trifurcate tributaries originating from typical agricultural catchments and flowing through a shared river network area (lower reaches), which is recognized as the fastest urbanizing regions globally, and eventually merging into the South China Sea through the Lingdingyang Estuary (Figure 1).[21] The exceptional characteristics of the Pearl River, including its intensive influence from irregular semidiurnal tides and the continuous formation of a noticeable riverine salinity gradient in the three tributaries, make it an ideal river system for comprehensive exploration of the intricate relationships between aquatic microbial communities and the bioavailability and transformation of DOM along the salinity gradient.[22]

In this study, we investigated the transformation reactions of DOM along the salinity gradient of the Pearl River (i.e., Upper Reaches, River Network Area, the Estuary Area, and the Ocean Area) using bioincubation experiments to assess potential microbial utilization and turnover of DOM by favorable microbial communities across different salinity levels. The 3D Excitation−Emission−Matrix Spectra combined with parallel factor analysis (EEM−PARAFAC) was exploited to trace the potential sources of DOM in different river reaches. The Fourier transform-ion cyclotron resonance mass spectrometry (FT−ICR MS) was utilized to comprehensively differentiate molecular signatures of DOM between pre- and postbiodegradation stages and further evaluate the changes in quantity and composition of DOM caused by characteristic microbial communities. We also employed 16S rRNA technology to investigate the abundance and diversity of characteristic aquatic microbial communities along the salinity gradient and explore the interaction between microbial diversity and DOM bioavailability using the co-occurrence network analysis between microbial operational taxonomic units (OTUs) and DOM molecules. This study provides insights toward the influence of the microbial community difference on the bioavailability and transformation of DOM along the salinity gradient in river−ocean continua.

2. MATERIALS AND METHODS

2.1. Site Description and Sample Collection. Water samples were collected from four different salinity-gradient

https://doi.org/10.1021/acsestwater.4c00832
ACS EST Water 2025, 5, 2096−2109

river reaches of the Pearl River, i.e., the Upper Reaches (three trifurcate tributaries: West River, WR, W1−W10; North River, NR, N1−N8; East River, ER, D1−D6), the River Network Area (the lower reaches, R1−R16), the Estuary Area (the Lingdingyang Estuary, E1−E8), and the Ocean Area (South China Sea, S1−S4) based on hydrologic and geographical characteristics (Figure 1). As the land use types of study areas shown in Figure 1, the sampling locations of the Upper Reaches were basically surrounded by forest (or grass) and agricultural areas, while the sites in the River Network Area were primarily located in urban regions. The collection of water samples was conducted in August 2023 for the summer period and in January 2024 for the winter period.

A Niskin bottle (10 L, sequentially pretreated by HCl solution with pH 2.0 and Milli-Q water) was employed to collect surface water samples. Water samples in the region of the continental shelf were collected from the surface (0−50 cm below the water surface) and bottom seawater (0−50 cm above the bottom). Typical parameters of water quality, i.e., salinity, pH, and oxidation−reduction potential (ORP), were determined in situ using a portable multiparameter probe (YSI ProDSS, USA) (Table S1). Triplicate salinity tests were conducted for each water sample, and the average salinity values are recorded in Table S1. Afterward, water samples were kept in dark ice incubators, transferred to refrigerator at 4 °C the same day as sample collection, and further analyses were conducted within 3 days. Total nitrogen (TN), total phosphorus (TP), and chemical oxygen demand (COD) of water samples are recorded in Table S1. All samples were characterized by the optical measurement.

2.2. Bioincubation Experiments. Bioincubation experiments were set up at once the water samples arrived at laboratory. First, the water samples (0.6 L) were filtered through Millipore membrane cellulose filters (0.45 μm), and then every 100 mL aliquot was filled in a 150 mL precombusted amber glass serum bottle with 50 mL of headspace. Afterward, 5 mL site-specific raw water filtered through 2.7 μm GF/D filters was spiked as bacterial inoculum into each serum bottle. For samples from the identical sampling location, three serum bottles were acidified by 2 mL of 50% H_3PO_4 at T = 0 days, and stored at 4 °C. The acidification was conducted to inhibit microbial activities in the water samples and ensure the accuracy of experimental results. Unacidified samples (n = 3) were kept in a dark incubator at 20 °C for 28 days. The bottle caps were opened and gently shaken several times a day to keep the samples oxygenated.

2.3. Dissolved Organic Carbon Concentration. Dissolved organic carbon (DOC) samples (T = 0 and 28 days) were measured by employing a total organic carbon analyzer (Shimadzu TOC−L, Japan). The bioavailable DOC (BDOC, mg C L^{-1}) was calculated by the average loss of DOC concentrations between T = 0 and 28 days during the bioincubation experiments (ΔDOC, eq 1):

$$\Delta\mathrm{DOC} = \mathrm{BDOC} = \frac{\mathrm{DOC}_0 - \mathrm{DOC}_{28}}{\mathrm{DOC}_0} \quad (1)$$

The UV−vis absorption spectra of water samples were obtained in the range of 200−800 nm with 1 nm interval by a UV-8000 spectrophotometer using Milli-Q water as a blank. $SUVA_{254}$ and a_{350} refer to the ratio of the absorbance coefficients at the wavelength of 254 nm to the DOC concentration and DOM absorbances at the wavelengths of 350 nm, respectively, which were employed as surrogates to trace the aromaticity of DOM and the concentrations of lignin components.[23,24] The spectral slope of DOM absorbance at 275−295 nm ($S_{275-295}$) tends to increase with the molecular size of DOM.[25] The 3D Excitation−Emission−Matrix (EEM) Spectra of DOM samples were obtained with a Hitachi F-7000 spectrofluorometer at room temperature (25 °C). The wavelength ranges of excitation (Ex) and emission (Em) were set to 220−450 nm with intervals of 5 and 240−600 nm with a wavelength step of 1 nm, respectively.

PARAFAC modeling was processed using R software (version 4.3.1, https://www.r-project.org/) for corrected EEM data after blank subtraction, Raman normalization, UV correction, and clipping of Raman Rayleigh scattering. Three fluorescence parameters, i.e., fluorescence index (FI), autochthonous index (BIX), and humification index (HIX), were employed as surrogates to trace the fluorescent DOM (FDOM) origins, biological activity, and humification degree, respectively. Their calculation methods are elaborated in Table S2.

2.4. Dissolved Organic Matter Molecular Composition. Agilent Bond Elut PPL (500 mg per 6 mL) was employed to desalt and concentrate DOM in water samples across the riverine salinity gradient by solid-phase extraction. Afterward, the extracted DOM samples were analyzed by a Bruker SolariX FT−ICR MS equipped with a 15.0 T superconducting magnet and negative electrospray ion (ESI) source (Bruker, Billerica, Massachusetts). Detailed information on FT−ICR MS procedures is provided in Text S1 in the Supporting Information.

Molecular formulas of DOM were identified from peaks exhibiting a signal-to-noise ratio (S/N) ≥4 using the Bruker Daltonics Data Analysis software based on stringent criteria with elemental combinations of $^{12}C_{1-60}$, $^{1}H_{1-120}$, $^{16}O_{1-50}$, $^{14}N_{0-5}$, and $^{32}S_{0-1}$, ensuring that the mass error between the measured mass and calculated mass for a given chemical formula was maintained below 0.5 ppm. The calculation methods of molecular parameters, i.e., double bond equivalent (DBE) and nominal oxidation state of carbon (NOSC), are provided in Text S1 in the Supporting Information. The weighted average value of all molecular-level parameters was calculated using the relative intensities (RIs) of each formula.[26] Based on the modified aromaticity index (AI_{mod}) and the ratios of H/C and O/C, DOM molecules were classified as five categories: (1) polyaromatic hydrocarbons (PAH, AI_{mod} > 0.66), (2) polyphenols (Polyph, 0.66 ≥ AI_{mod} > 0.50), (3) highly unsaturated and phenolic compounds (HuPh, AI_{mod} ≤ 0.50 and H/C < 1.5), (4) unsaturated aliphatic compounds (Aliph, AI_{mod} ≤ 0.50 and 2.0 > H/C ≥ 1.5), and (5) carbohydrate compounds (Carbo, AI_{mod} ≤ 0.50 and H/C ≥ 2.0).[27] Based on molecular size fractions, DOM molecules were divided into three categories: low-Mw DOM (<300 Da), medium-Mw DOM (300−500 Da), and high-Mw DOM (>500 Da).[28]

3. RESULTS AND DISCUSSION

3.1. Spectroscopic Characteristics and Bioavailability of DOM along the Salinity Gradient. With the tidal movement of the South China Sea, the salinity of the Pearl River shows a clear increasing gradient from the Upper Reaches (i.e., three trifurcate tributaries: North River, 0.05 ppt; East River, 0.05 ppt; and West River, 0.09 ppt) to the River Network Area (0.50 ppt), then to the Estuary (3.18 ppt), and

https://doi.org/10.1021/acsestwater.4c00832
ACS EST Water 2025, 5, 2096−2109

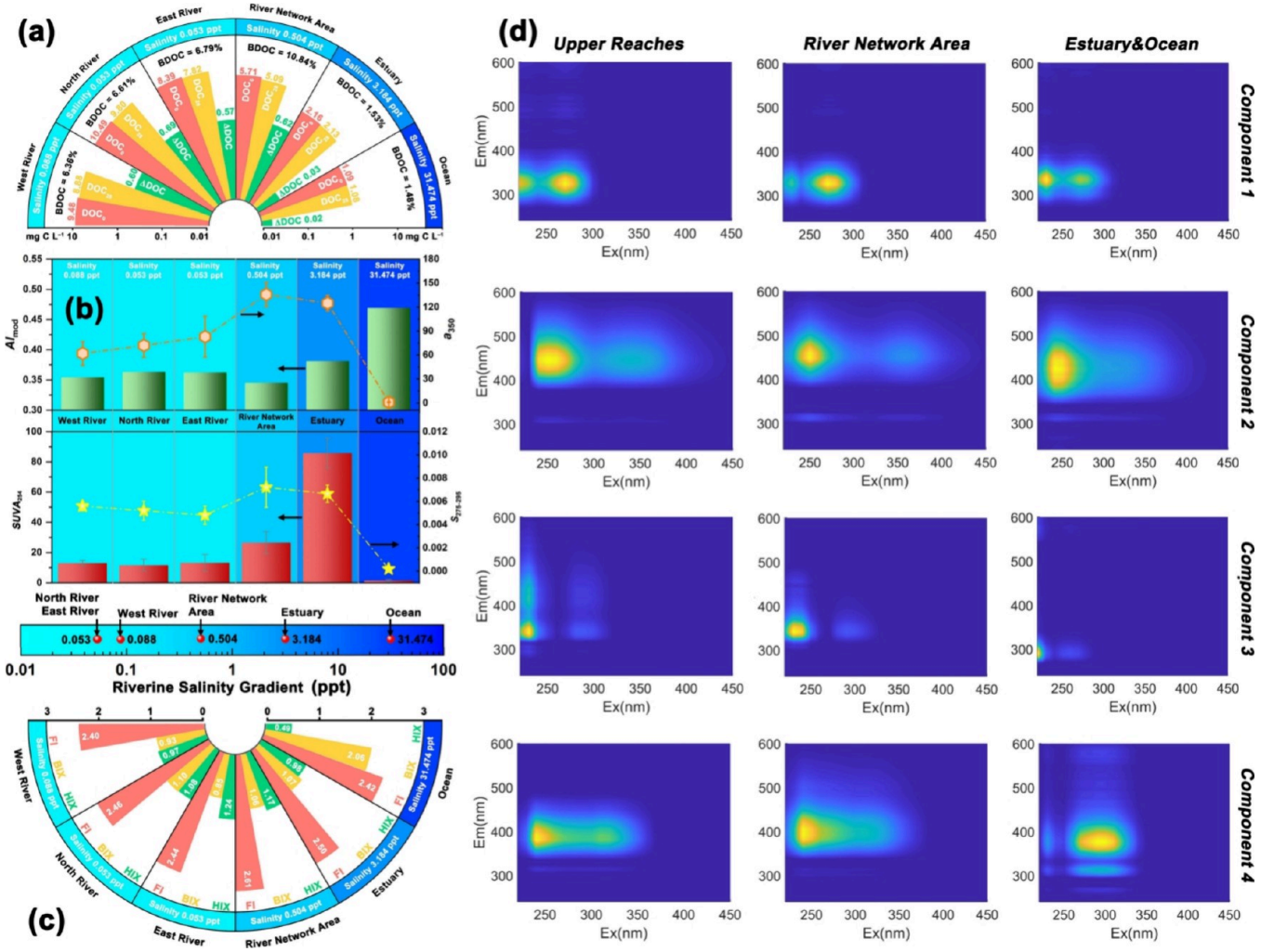

Figure 2. Spectroscopic characteristics and bioavailability of DOM along the riverine salinity gradient. (a) Variations of DOC_0, DOC_{28}, ΔDOC, and bioavailable DOC (%BDOC); (b) variations of AI_{mod}, a_{350}, $SUVA_{254}$, and $S_{275-295}$; (c) variations of FI, BIX, and HIX; and (d) fluorescence components obtained using the EEM−PARAFAC model.

finally to the Ocean (South China Sea, 31.47 ppt) (Figure 2). Additionally, Figure 2a−c demonstrates that, along the salinity gradient, DOM forms a regular distribution fingerprint. DOC_0 exhibits an obvious decreasing trend in Figure 2a (North River, 10.49 mg C L^{-1}; East River, 8.39 mg C L^{-1}; West River, 9.48 mg C L^{-1}; River Network Area, 5.71 mg C L^{-1}; Estuary, 2.16 mg C L^{-1}; and Ocean, 1.09 mg C L^{-1}). It is noteworthy that BDOC presents a trend of initially increasing and then decreasing with the change in salinity. It ranges between 6 and 7% in the Upper Reaches (North River, 6.61%; East River, 6.79%; and West River, 6.36%), significantly increases in areas of high urbanization, such as the River Network Area (10.84%, $p < 0.01$) where human activities are intensive (Figure 1), and finally drops to 1.53% in the Estuary and 1.48% in the Ocean. This indicates that autochthonous (e.g., algae and phytoplankton) and anthropogenic DOM (e.g., fertilizers, excreta, and wastewater) generated by local urbanization are more readily bioavailable, further supported by significantly reduced H/C ratios ($p < 0.01$) after biodegradation in the River Network Area (Figure 3 and Figure S1).[8]

Figure 2b depicts that the optical properties of DOM show a relatively obvious spatial difference along the riverine salinity gradient. a_{350} as an indicator characterizing the lignin component exhibits a trend of increasing initially and then decreasing with the rise in river salinity, reaching its peak in highly urbanized River Network Area (135.8 m^{-1}), and gradually decreases to 0.98 m^{-1} in the Ocean. This may be associated with the large-scale use of wood in urban construction.[29] As a characteristic terrestrial DOM, lignin (a_{350}) gradually decreases during its transport and transition to the ocean.[30] However, the variation in AI_{mod} (modified aromaticity index) presents an almost opposite trend, being lowest in the River Network Area (0.34) and reaching its peak of 0.47 in the Ocean. This is related to the increasing trend of DOM with high aromaticity (i.e., PAH and Polyph) along the river flow (Figure 3).

Figure 2c,d illustrates fluorescence characteristics of DOM along the salinity gradient. All FI values are distributed between 2.40 and 2.61, indicating that the humic substances from the Upper Reaches to the Ocean are primarily composed of autochthonous DOM.[31,32] This demonstrates the dominant role of microbial activity in the transformation of DOM within this river−ocean system.[32] Across different salinity gradient, the Ocean exhibits the lowest HIX and highest BIX. This suggests that microbial activity in this area is more vigorous, playing a significant role in the formation and transformation

https://doi.org/10.1021/acsestwater.4c00832
ACS EST Water 2025, 5, 2096−2109

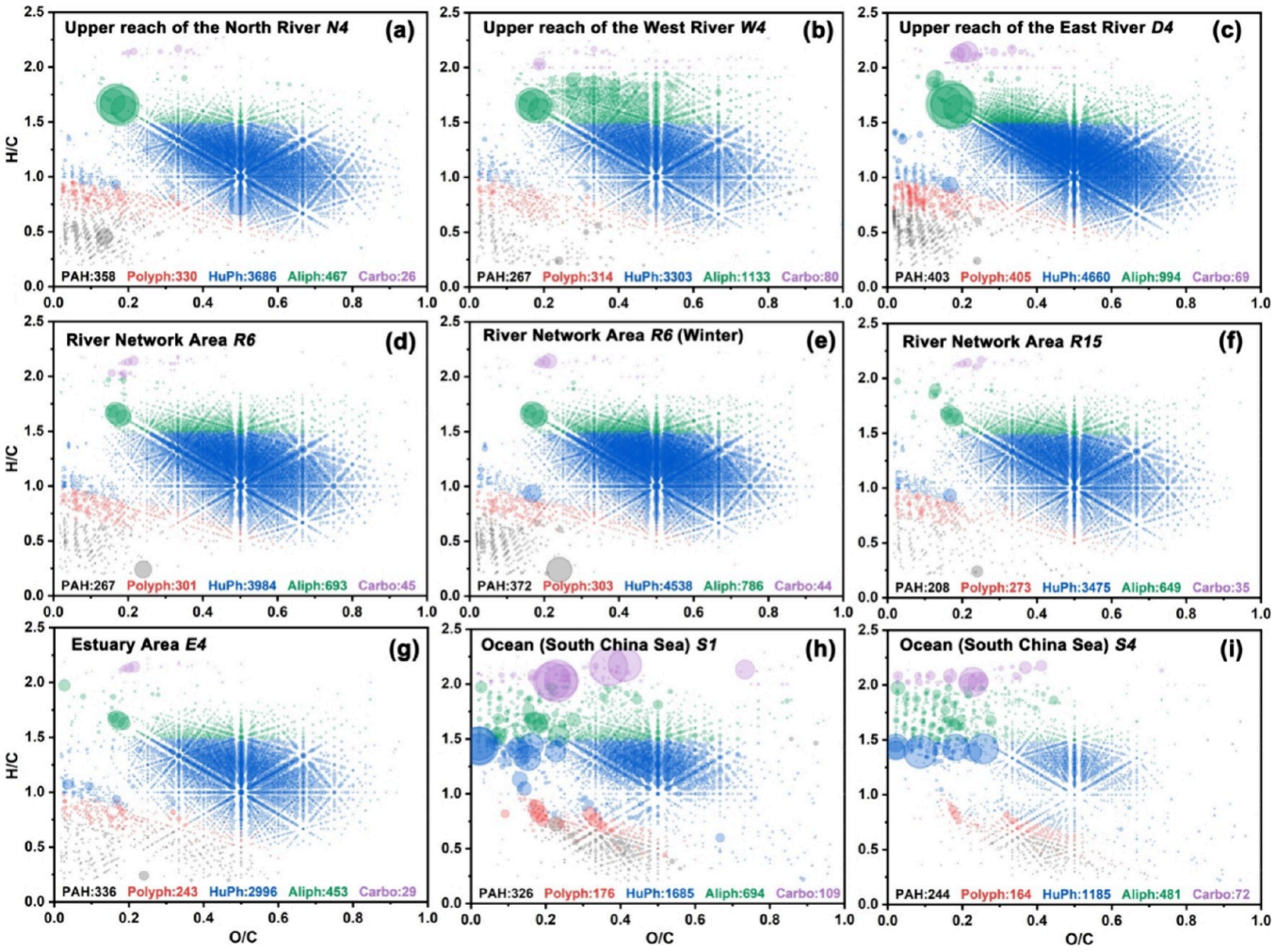

Figure 3. Van Krevelen diagrams describing the DOM formulas (before bioincubation experiments) in (a) Upper Reach of the North River N4, (b) Upper Reach of the West River W4, (c) Upper Reach of the East River D4, (d) River Network Area R6, (e) River Network Area R6 in winter, (f) River Network Area R15, (g) Estuary Area E4, and (h) Ocean (South China Sea) S1, and (i) Ocean (South China Sea) S4. A larger dot size represents the higher relative intensities of the molecules in the DOM. The numbers at the bottom of the figure represent the number of molecules in different components.

of DOM.[33,34] Furthermore, the DOM is primarily autochthonous and recently produced.[33,34] The detailed explanation and analyses of fluorescence components using the EEM−PARAFAC model in Figure 2d are shown in Table S3 in the Supporting Information.

3.2. Compositional Changes and Molecular Transformation of DOM. Figure 3 and Figure S2 illustrate the compositional changes of DOM before and after biodegradation by salinity-differentiated microbial communities, and detailed molecular information along salinity gradient is summarized in Tables S4−S6. DOM molecules with molecular weights (Mw) ranging from 300 to 800 Da are taken into consideration. Based on molecular size fractions, DOM molecules were divided into three categories: low-Mw DOM (<300 Da), medium-Mw DOM (300−500 Da), and high-Mw DOM (>500 Da). In the Upper Reaches (i.e., N4, D4, and W4), DOM is primarily composed of Medium- and High-Mw DOM, accounting for 45.05 and 42.54%, respectively (Figure 3a−c and Table S4). However, after biodegradation, the proportion of high-Mw DOM decreases to 31.42%, a reduction of 13.63%, while the medium- and low-Mw DOM increase to 53.61 and 14.97%, respectively. This indicates a transformation process of high-Mw DOM to medium- and low-Mw DOM under microbial decomposition at salinities between 0.03 and 0.15 ppt. The average Mw decreased from 474.64 to 437.18 Da, further substantiating this point. Simultaneously, this trend was also observed in the River Network Area (salinity 0.15−4.23 ppt) and the Estuary and Ocean Areas (salinity 4.58−43.72 ppt) (Figure 3d−h and Tables S4 and S5). Contrarily, in the River Network Area and the Estuary and Ocean Area, the initial proportions of high-Mw DOM are comparatively lower, only 34.88 and 37.57% and the decreases are only 7.24 and 6.36%, respectively. The proportion of high-Mw DOM is consistent with the DOM bioavailability in different areas (as concluded in Section 3.1). In the highly urbanized River Network Area, the proportion of large molecular DOM is relatively the lowest with strongest bioavailability. This could potentially be due to the fact that local DOM inputs (e.g., fertilizers, excreta, and wastewater) are more likely to have already undergone intense microbial degradation.[11]

HuPh and Aliph, as the 2 dominant DOM categories, account for 70.62 and 15.73% in the Upper Reaches, 75.11 and 13.32% in the River Network Area, and 63.81 and 17.71% in the Estuary and Ocean Areas, respectively (Figure 3 and

https://doi.org/10.1021/acsestwater.4c00832
ACS EST Water 2025, 5, 2096−2109

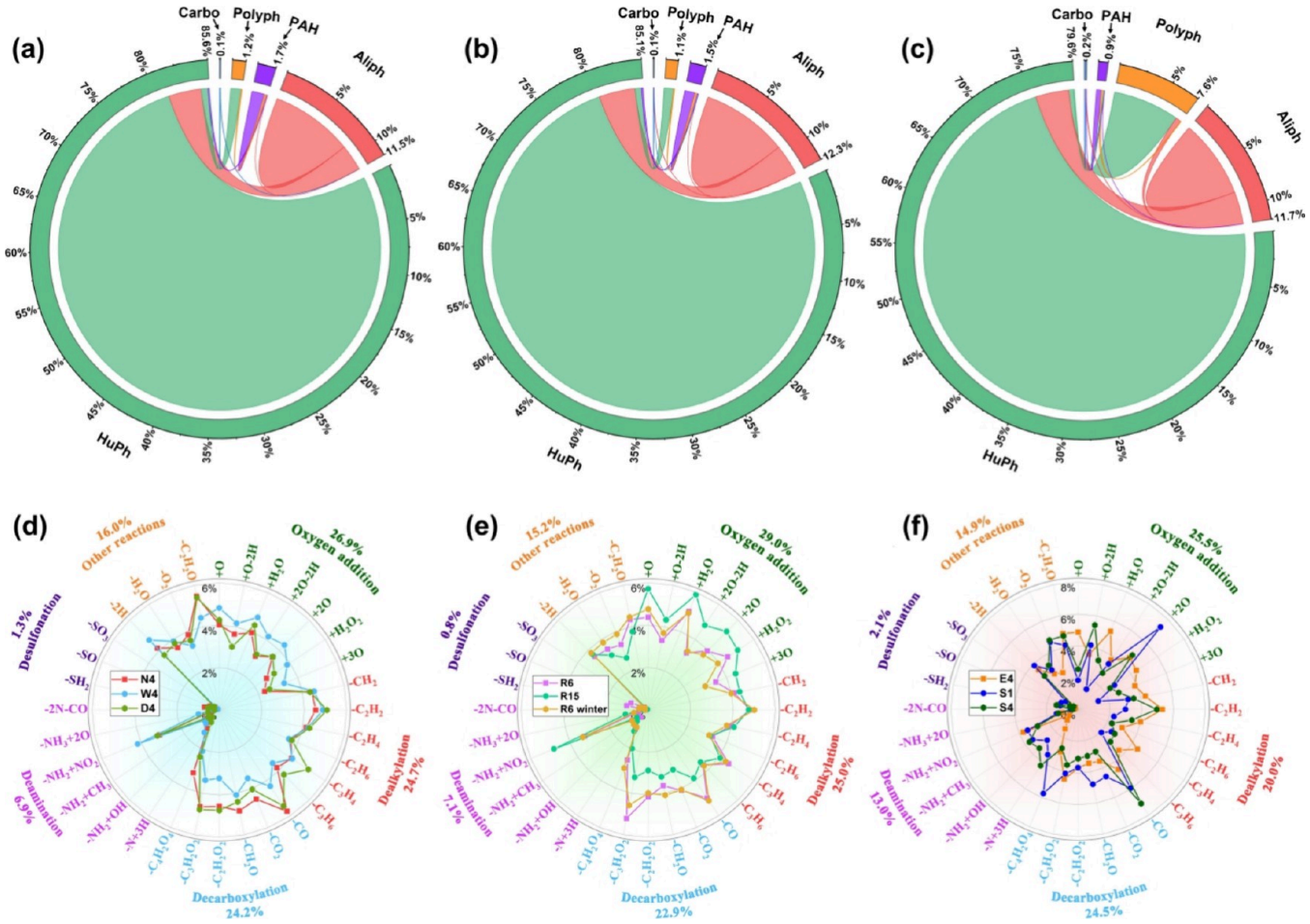

Figure 4. Chord diagrams show potential transformations in different salinity-gradient river reaches: (a) Upper Reaches (salinity = 0.03−0.15 ppt); (b) River Network Area (salinity = 0.15−4.23 ppt); and (c) Estuary and Ocean Areas (salinity = 4.58−43.72 ppt); and Radar plots of possible linkages based on the 32 reactions during biodegradation in different salinity gradients: (d) Upper Reaches (salinity = 0.03−0.15 ppt); (e) River Network Area (salinity = 0.15−4.23 ppt); and (f) Estuary and Ocean Areas (salinity = 4.58−43.72 ppt).

Tables S4−S6). Microbial communities differentiated by varying salinities exhibit entirely distinct transformation effects on different types of DOM during the biodegradation process. For instance, the proportion of HuPh only decreases by 4.67% in the River Network Area after microbial transformation, while it increases by 3.69 and 2.11% in the Upper Reaches and the Estuary and Ocean Areas, respectively. PAH, as micropollutants with potent toxicity and carcinogenicity to both humans and aquatic organisms,[35] constitutes as much as 6.23% of the DOM in the Upper Reaches, 5.30% in the River Network Area, and increase to 9.86% in the Estuary and Ocean Areas. After microbial transformation, the proportion of PAH in the densely populated River Network Area increases by 2.47−7.77%, while it decreases by 0.13 and 2.94% in the River Network Area and Estuary and Ocean Areas, respectively. Simultaneously, the potential biochemical transformations between DOM molecules, as depicted in Figure 4a−c and Table S7, further substantiate distinct transformation effects of DOM under the influence of salinity-differentiated microbial activities in different areas, particularly in the Estuary and Ocean Areas. Most notably, the transformation from Aliph to HuPh in the Estuary and Ocean Area is markedly more intense (6.94%) compared to other areas (1.08% for the Upper Reaches and 0.99% for the River Network Area) (Figure 4c), suggesting that microbes in high-salinity seawater exhibit a stronger propensity to induce the transformation of aliphatic DOM toward a highly unsaturated phenolic state.[27]

CHO compounds predominate in all three areas, yet they gradually decreases with the increase in salinity (50.06% for the Upper Reaches, 47.51% for the River Network Area, and 44.11% for the Estuary and Ocean Areas) (Tables S4−S6). Simultaneously, there is a noted incremental rise in N-containing DOM (i.e., CHON and CHONS) compounds along with the salinity gradient (36.17% for the Upper Reaches, 39.92% for the River Network Area, and 47.06% for the Estuary and Ocean Areas). This increase becomes more pronounced with increasing salinity, indicating a differential accumulation of N by microbes under varying salinities. Specifically, as salinity increases, the efficiency of N accumulation intensifies. This conclusion is in accordance with the findings presented in Section 3.4, which exhibits a significant positive correlation between salinity and the N content in the river−ocean continuum. Sulfur-containing DOM (i.e., CHOS and CHONS) shows little to no substantial changes (18.08% for the Upper Reaches, 18.39% for the River Network Area, and 16.90% for the Estuary and Ocean Areas).

3.3. Possible Reactions during Salinity-Related Biotransformation. The substantial alterations at the molecular level of DOM suggest that a multitude of reactions transpired during biotransformation, induced by the salinity-differentiated

https://doi.org/10.1021/acsestwater.4c00832
ACS EST Water 2025, 5, 2096−2109

microbial community across various areas. Figure 4d−f depicts the linkage analysis based on the 32 most probable reactions (Table S8), which are categorized into six major types: oxygen addition, dealkylation, decarboxylation, deamination, desulfonation, and other reactions.[36] This analysis is conducted to elucidate the differential interactions induced by salinity-differentiated microbial community during the biotransformation of DOM. Across the three areas differentiated by salinity, oxygen addition emerges as the most potent reaction type (26.9% for the Upper Reaches, 29.0% for the River Network Area, and 25.9% for the Estuary and Ocean Area). However, reactions involving oxygen removal (e.g., decarboxylation, 24.2, 22.9, and 24.5%; other reactions, 16.0, 15.2, and 14.9%, respectively) are also notably strong. Consequently, the O/C ratio of DOM in each area remains basically unchanged following the reactions (Tables S3−S6, $\Delta O/C$ = 0.01−0.01 and 0.01%, respectively). During the microbial transformation process across different salinity levels, there are similarities in DOM changes across three areas. For instance, the desulfonation reaction is consistently weak (1.3% for the Upper Reaches, 0.8% for the River Network Area, and 2.1% for the Estuary and Ocean Areas, $p > 0.05$), while the $-C_2H_2$ and −CO reactions are invariably strong. Presumably due to the minor variations in salinity between the Upper Reaches and River Network Area (Table S1), their reactions exhibit greater similarity ($p > 0.05$). For instance, in the deamination reactions, only the $-NH_2 + NO_2$ reaction is pronounced (3.46% for the Upper Reaches and 3.79% for the River Network Area), while the others are considerably weak (<1%). Conversely, in the Estuary and Ocean Areas, all deamination reactions, with the exception of −2N−CO (0.36%), have a relatively high reaction proportion (3.31% for $-NH_2 + NO_2$, 3.05% for −N + 3H, 2.58% for $-NH_2 + CH_3$, 2.39% for $-NH_2$ + OH, and 1.22% for $-NH_3$ + 2O). Hence, the deamination reaction in the Estuary and Ocean Areas significantly surpasses that in the other 2 areas, reaching as high as 13.0%. Of particular note is our investigation into the differences in the reaction transformation pathways of DOM in the highly urbanized River Network Area R6 during summer (salinity = 0.23 ppt, T = 35.2 °C) and winter (salinity = 0.35 ppt, T = 9.3 °C). The results reveal an insignificant difference ($p > 0.05$) in the proportions of each transformation reaction mediated by microbes in summer and winter, indicating that temperature is not the main factor affecting the types of DOM microbial transformation reactions (Figure 4e). When combined with the reaction type disparities at other sampling points in distinct salinity areas, it suggests that the differences in microbial communities under salinity differentiation may be the source of the differences in DOM reaction transformation pathways (Figure 4d−f).[12,16]

In the process of DOM transformation, concerning precursors (relative intensities decreased by more than 30%), resistants (relative intensity changes of less than 30%), and products (relative intensities increased by more than 30%), approximately 70% of DOM behaved as precursors across the 3 salinity areas (71.4% for the Upper Reaches, 72.5% for the River Network Area, and 66.6% for the Estuary and Ocean Area) (Table S2). Across the three areas, the quantity of products is invariably less than that of precursors. However, the ratio of precursors to products exhibits a clear trend of increasing with salinity (products/precursors = 16.9, 27.2, and 36.5% for the Upper Reaches, the River Network Area, and the Estuary and Ocean Areas, respectively). This suggests that the microbial transformation process in the Upper Reaches and its products tend to be more homogeneous, indicating a stronger selectivity in the DOM transformation by the microbial community differentiated by low salinity.[30] Conversely, the microbial transformation in the Estuary and Ocean Areas and its products tend to be more diverse, suggesting that the microbial community differentiated by high-salinity water environments has a broader range in the degradation and transformation of DOM.[36] On the other hand, this indirectly indicates that microbial activity in the high-salinity marine environment is more vigorous.[36] This finding aligns with the conclusion in Section 3.1 regarding the high BIX in this area (Figure 2c).

To gain a deeper understanding of the molecular characteristics of precursors, resistants, and products under different salinity conditions, we have classified them into five categories (PAH, Polyph, HuPh, Aliph, and Carbo) based on their chemical composition, as shown in Tables S9−S11. It is evident that within three distinct salinity areas, high-Mw DOM (>500 Da) is the dominant component of precursors (50.7% for the Upper Reaches, 45.6% for the River Network Area, and 59.0% for the Estuary and Ocean Areas) and products (51.9, 50.7, and 56.9%, respectively), while resistants are primarily associated with medium-Mw DOM (300−500 Da; 60.2, 51.9, and 56.3%, respectively). A plausible explanation for this phenomenon lies in the hypothesis that these medium-Mw DOM species represent a transitional state in the continuum from high-Mw molecules to low-Mw ones.[26] The degradation rate and formation rate of these intermediate DOM constituents might reach an equilibrium, thereby imparting an apparent enhanced resilience against microbial degradation compared to their extremal counterparts in terms of molecular size.[26] This balance suggests a nuanced interplay between the production and consumption of DOM fractions within the ecosystem, highlighting the dynamic nature of DOM transformation processes. Interestingly, the proportion of Polyph ($0.66 \geq AI_{mod} > 0.50$) among the low-Mw resistants in various regions is notably high (39.9% for the Upper Reaches, 48.2% for the River Network Area, and 40.4% for the Estuary and Ocean Areas), whereas the presence of PAH ($AI_{mod} > 0.66$), theoretically more recalcitrant to microbial degradation, is comparatively lower (Tables S9−S11). This discrepancy may stem from a higher proportion of PAH resistants being associated with medium-Mw and high-Mw DOM (75.9, 73.4, and 82.2%, respectively), the precursors of low-Mw ones.[37] Of particular note, in the River Network Area, all five distinct categories of DOM exhibit varying degrees of increase in the Avg Mw of their products compared to their precursor counterparts (Tables S9−S11). Conversely, in the Estuary and Ocean Areas, a uniform decrease is observed. The Upper Reaches present a more nuanced picture, where only Carbo and Polyph show an increase, while the rest (i.e., Aliph, HuPh, and PAH) undergo a decline. This further corroborates the hypothesis that salinity-differentiated microbial populations play a pivotal role in mediating variations in DOM transformation effects. Furthermore, with respect to compositional changes in DOM during transformation, the bioavailability of sulfur to microbial communities varies across different areas, characterized by a decline and then a rise in the CHOS and CHONS ratios within precursors, progressing from the Upper Reaches (37.3%) through the River Network Area (32.8%) to the Estuary and Ocean Area (43.7%). It is noteworthy that in both the Upper Reaches and Estuary and Ocean Areas, the

https://doi.org/10.1021/acsestwater.4c00832
ACS EST Water 2025, 5, 2096−2109

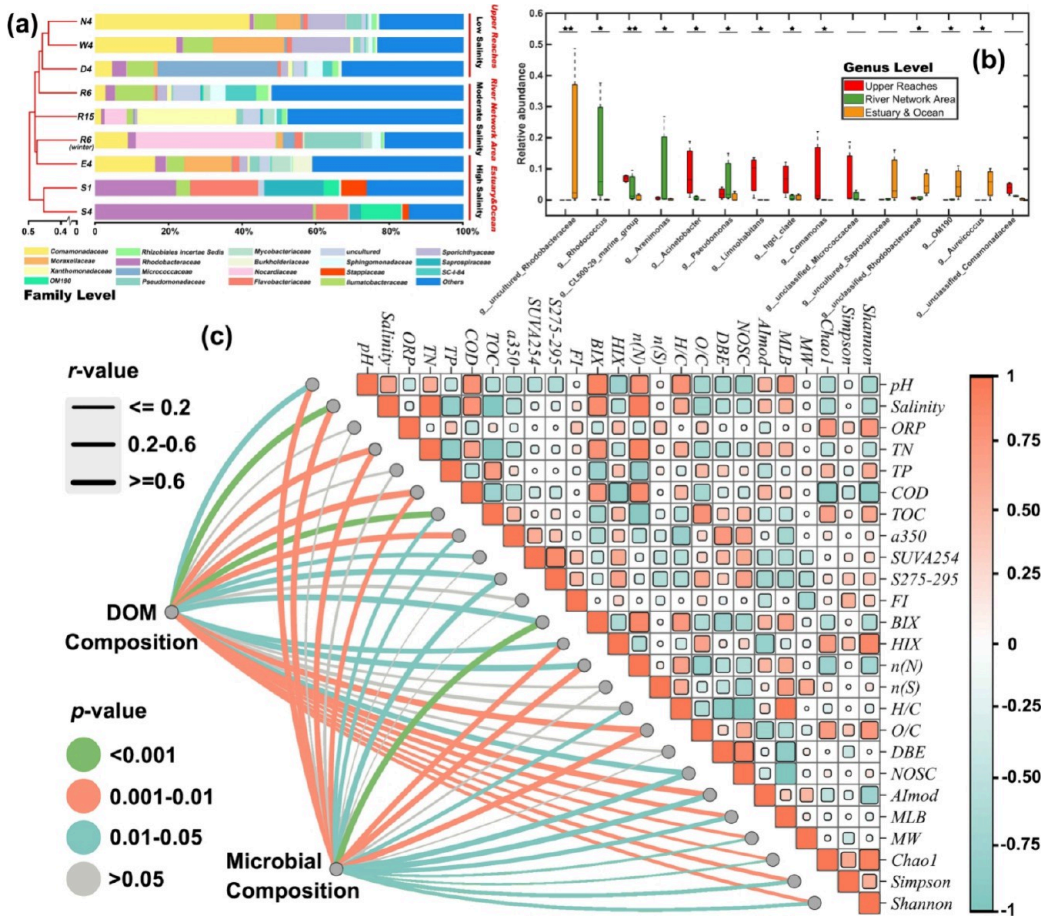

Figure 5. (a) Cluster analysis of microbial communities at the family level along the riverine salinity gradient. (b) Kruskal–Wallis H test box plot shows the top nine genera in abundance at the genus level. Genera with significant differences were labeled with * ($p < 0.05$) and ** ($p < 0.01$). (c) Mantel test-based correlations between microbial and DOM composition with parameters. Mantel's r value is represented by the edge width, and the statistical significance p is represented by the color. Pairwise Spearman's coefficients between parameters are shown with a color gradient.

Carbo (H/C > 2.0) of CHO within DOM achieves full conversion, evidenced by resistants of 0% (Tables S9 and S11). This observation indirectly underscores the significance of a high H/C in DOM as a facilitator of its microbial degradability.[8]

3.4. Microbial Composition and Distribution along the Salinity Gradient. Initially, cluster analysis was conducted based on the outcomes of 16S rRNA gene sequencing (Figure 5a). The aquatic microbiota was distinctly segregated into two clusters: one extending from the Upper Reaches and River Network Area to the Estuary Area, and the other inhabiting the Ocean Area. Notably, within the first cluster, a marked gradational shift in microbial clustering was observed in accordance with increasing salinity levels (Figure 5a). The microbial communities of the Upper Reaches of the North River (N4) and West River (W4) exhibited the highest degree of proximity, a phenomenon potentially attributable to the hydrological connectivity between these two tributaries.[14] Closely following was the Upper Reach of East River (D4), also characterized by low-salinity conditions. As salinity rose, these clusters progressively aligned with those of R6, R15, and E4. Of particular interest is the finding that the microbial assemblage sampled at R6 during winter showed a higher resemblance to summer samples from E4 in the Estuary Area. This observation underscores the impact of reduced precipitation in winter, which facilitates the intrusion of saltwater upstream, on the microbial ecosystem dynamics of the riverine environment.[13−15]

At the family level, an important microbial population shared across sites at low- and moderate-salinity levels was *Comamonadaceae* (14.2% ± 14.3%) (Figure 5a), exhibiting a tendency that initially decreased from the Upper Reaches toward the River Network Area before increasing again toward the Estuary Area along the salinity gradient. Specifically, *Micrococcaceae* dominated at D3 (32.6%), while *Ilumatobacteraceae*, *Xanthomonadaceae*, and *Moraxellaceae* were the predominant taxa at sites R6 (10.3%), R15 (26.9%), and E4 (12.9%), respectively. Notably, the microbial community at R6 during winter bridged the characteristics of R15 and E4, with a population structure resembling E4 in terms of the ratio of *Rhodobacteraceae* to *Comamonadaceae* (24.0 and 17.4%), and similarly featured a substantial presence of *Nocardiaceae*. In the Ocean Area, the predominant microbial population is composed predominantly of members belonging to the *Rhodobacteraceae* family (22.0% for S1 and 59.2% for S4).

A majority among the foremost 15 bacterial genera displayed significant variations across three distinct salinity areas ($p < 0.05$), highlighting notable differences in the composition of the major microbiota among these environments and their differential response to salinity gradients (Figure 5b). Additionally, the investigation uncovered a considerable diversity of known functionally relevant genera. *Rhodococcus*, *Arenimonas*,

https://doi.org/10.1021/acsestwater.4c00832
ACS EST Water 2025, 5, 2096−2109

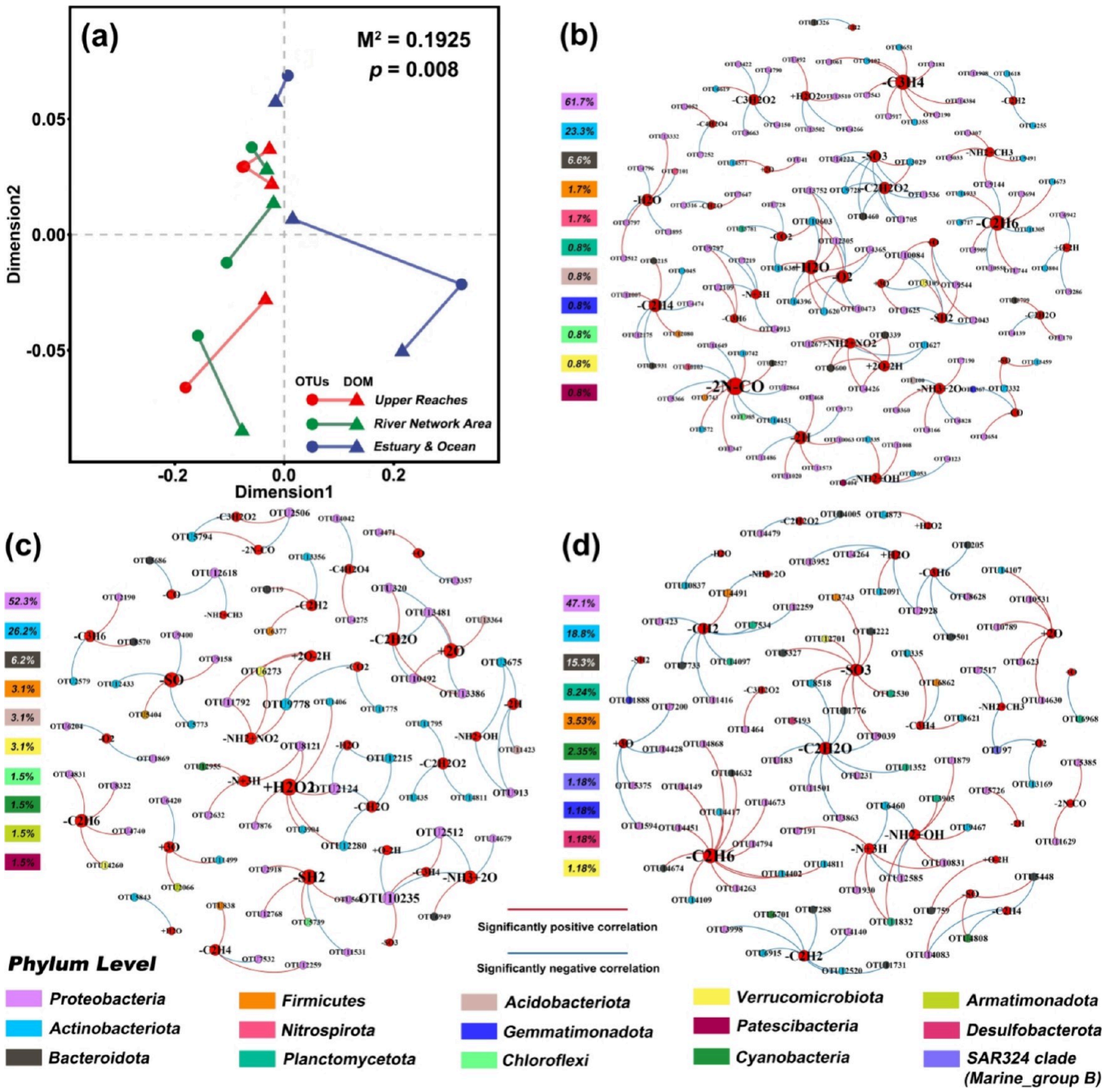

Figure 6. (a) Procrustes analysis between the DOM composition and microbial composition. The results (M^2 = 0.1925, p < 0.01) indicate that DOM and microbial communities are closely correlated. (b–d) Co-occurrence network analysis between microbial OTUs and DOM transformation reactions in the Upper Reaches, the River Network Area, and the Estuary and Ocean Areas, respectively.

Acinetobacter, *Pseudomonas*, *Limnohabitans*, and *Comamonas* play crucial roles in denitrification.[38−42] *Limnohabitans* contributes to DOM sulfur oxidation,[41] while *Comamonas* uniquely features DOM deacetylation.[42] Among these, *Acinetobacter*, *Limnohabitans*, and *Comamonas* genera are predominantly found in the low-salinity Upper Reaches, whereas *Rhodococcus*, *Arenimonas*, and *Pseudomonas* are mainly concentrated in the moderate-salinity River Network Area. The primary microbial constituents in the Estuary and Ocean Area are representatives of the *Rhodobacteraceae* family, primarily known for their roles in photosynthesis and nitrogen fixation.[43−45] In comparison, high salinity in Estuary and Ocean Areas may lead to a reduction in the population of denitrifying bacteria (Figure S3).

3.5. Relationships between Microbial Community and DOM Composition. To evaluate the impact of external environmental factors on the microbial community structure and molecular DOM composition, a Mantel test was employed (Figure 5c). Among all parameters examined, significant strong correlations were identified between both the DOM composition and microbial community with salinity levels (r > 0.60, p < 0.01), affirmatively implicating salinity as a key regulator in the structuring of DOM and its microbial-mediated transformations.[12,16] Additionally, a significant positive association emerged between salinity and the N

https://doi.org/10.1021/acsestwater.4c00832
ACS EST Water 2025, 5, 2096−2109

content (i.e., TN and n(N)) of DOM, with a correlation coefficient exceeding 0.95 ($p < 0.001$). This finding may be linked to a reduction in the population of denitrifying bacteria as salinity levels rise.[43] Conversely, TOC and TP displayed significant negative correlation with salinity ($r = -0.95$ and $p < 0.001$ for TOC, and $r = -0.83$, and $p < 0.01$ for TP). Collectively, these results emphasize salinity as a critical determinant underlying the variable microbial element utilization patterns and cycling dynamics in these aquatic systems. Meanwhile, a significant and robust correlation is also observed between salinity and both BIX ($r = 0.83$, $p < 0.001$) and the H/C ratio ($r = 0.64$, $p < 0.01$), implying that in higher salinity conditions, there is heightened microbial activity and a greater susceptibility of DOM to microbial degradation.[46] Based on these findings, it can be inferred that while an increase in salinity may decrease the number of nitrifying bacteria, it overall enhances the activity of other microorganisms involved in DOM degradation. This finding aligns with the preceding results, reinforcing the results that salinity exerts an important influence on the dynamics of microbial metabolism and DOM bioavailability.[46] To examine the correspondence in spatial ordering between DOM and the structure of water microbial communities, a Procrustes analysis was conducted (Figure 6a). This analysis amplified the viewpoint of a tight coupling between alterations in DOM characteristics and the microbial population dynamics, as evidenced along the salinity gradient ($M^2 = 0.19$, $p < 0.001$).

To elucidate more comprehensively the microorganismal specialization in DOM transformations, the analysis of co-occurrence network was conducted, providing mechanistic insights into the potential influence of microbial activity on DOM transformation pathways. Initially, through correlation analyses, 152, 88, and 98 OTUs were found to be significantly associated with DOM reaction types (Section 3.3) in the Upper Reaches, River Network Area, and the Estuary and Ocean Areas, respectively (Figure 6b–d). Despite the distinct OTU compositions observed in each of the three areas due to the modulatory effects of variables like salinity, a commonality at the phylum level was evident, with *Proteobacteria* (61.7, 52.3, and 47.1%), *Actinobacteriota* (23.3, 26.2, and 18.8%), and *Bacteroidota* (6.6, 6.2, and 15.3%) collectively representing the three dominant microbial communities across all investigated areas.

In conjunction with the depiction of 32 unique DOM transformation reactions under three salinity conditions in Figure 4d–f, the central red dots in Figure 6b–d symbolize the categories of DOM reactions, surrounded by points signifying the affiliated OTUs. Notably, in the Upper Reaches, 73 OTUs are implicated in enhancing DOM reactions, counterbalanced by 79 OTUs that appear to inhibit them. In River Network Area, this balance is maintained with 42 facilitative and 46 inhibitory OTUs. Likewise, in Estuary and Ocean Areas, 51 and 47 OTUs, respectively, exert promotional and suppressive influences, highlighting a discernibly equitable distribution of microbial activities that both foster and restrain DOM transformation reactions.[8]

Of particular note, the co-occurrence network analysis unveiled intriguing findings where identical OTUs were found to dominate disparate DOM transformation reactions under the sway of varying salinity conditions. OTU12259 illustrates an instance of this variability: In moderate-salinity conditions of the River Network Area, it significantly enhances dealkylation reactions ($-C_2H_4$), whereas in high salinity of the Estuary and Ocean Areas, it exerts a substantial inhibitory effect on a homologous reaction ($-CH_2$) (Figure 6c,d). Similarly, OTU14811 inverses its role from being a prominent inhibitor of $-C_2H_2O_2$ reactions in the River Network Area to a strong promoter of a different subset of $-C_2H_6$ reactions in the high-salinity Estuary and Ocean Areas. OTU335 manifests a discernible shift in its functional role: while it significantly fosters deamination reactions ($-NH_2 + OH$) in the low-salinity Upper Reaches, it subsequently promotes dealkylation reactions ($-C_3H_6$) when encountered in the high-salinity Estuary and Ocean Areas.

Within the identical salinity areas, the metabolism of select DOM species often necessitates the cooperative action of various microbial OTUs, underscoring that intricate macromolecular structures are seldom fully decomposed by a solitary microorganism, but rather through synergistic interactions within the microbial community.[47] For instance, in the Upper Reaches with low salinity, *Proteobacteria* strains OTU12677 and OTU4426, along with *Bacteroidota* members OTU3600 and OTU3339, collectively enhance the dominant deamination reaction $-NH_2 + NO_2$ (Figure 4d), exhibiting a significant positive correlation (Figure 6b). Simultaneously, under the influence of a shared salinity environment, microbial populations that facilitate certain DOM transformations exert a contrasting inhibitory effect on DOM reactions, thereby establishing a reciprocal pattern of enhancement and suppression. Specifically, OTU8518 of the *Actinobacteriota* phylum, OTU11776 from *Bacteroidota*, and OTU9039 belonging to *Proteobacteria*, while demonstrating a significant positive correlation with $-SO_3$ in desulfonation reactions in the high-salinity Estuary and Ocean Areas, concurrently exhibit a significant negative correlation with $-C_2H_2O$ in decarboxylation processes, exemplifying this intricate interplay of microbial regulation in DOM dynamics (Figure 6d). Notably, microorganisms from the phylum *Actinobacteriota* exhibit a predominantly inhibitory response to DOM reactions (70.0%) in the River Network Area of moderate salinity, whereas they demonstrate a mainly facilitative effect in other salinity conditions (57.9% for the Upper Reaches and 61.1% for Estuary and Ocean Areas) (Figure 6b–d). This further elucidates the disparity in microbial degradation behavior toward DOM under varying salinity areas. Moderate salinity might stimulate phylum *Actinobacteriota* to generate more extracellular polymeric substances (EPS), forming intricate networks that shield DOM from enzymes, reducing DOM transformations.[48,49] Alternatively, *Actinobacteriota* metabolism could chemically modify DOM, altering its structure to form more stable compounds, thereby impacting DOM processing.[49] This highlights the intricate interplay between salinity-mediated stress responses and the differential modulation of microbial activities in the DOM transformation cascade.

4. ENVIRONMENTAL IMPLICATIONS

The cellular osmotic pressure disparities induced by a salinity difference in river–ocean continua result in great variations in microbial community along the salinity gradient. However, understanding the DOM transformation and microbial responses in river–ocean continua at the molecular level remains a significant challenge. We selected the continuum of the Pearl River and South China Sea (salinity = 0.03–43.72 ppt) to comprehensively examine the molecular characteristics of DOM transformation reactions by microbial communities under the stress of salinity gradients using FT-ICR MS. Results

https://doi.org/10.1021/acsestwater.4c00832
ACS EST Water 2025, 5, 2096–2109

show that microbial activity intensifies with increasing salinity, especially DOM deamination reactions. However, the total N steadily rises with salinity, which aligns with the salinity-dependent inhibition of denitrifying bacteria. This result demonstrates the mediating role of salinity in the direction of DOM transformation. Simultaneously, compared with the Upper Reaches, although high urbanization in the River Network Areas has a significant impact on the composition and availability of DOM, it has a little effect on the type and proportion of DOM reactions. The influence mainly originates from the salinity-differentiated microbial populations. Notably, the saltwater intrusion during winter causes the microbial community structure in the River Network Area (salinity = 0.23 ppt in summer and 0.35 ppt in winter) to resemble more closely that of the Estuary Area in summer (salinity = 5.06 ppt), while the DOM transformation remains largely unchanged. This result clearly demonstrates that, although microbes dominate the transformation process of DOM, salinity can govern the microbe performance in this process, causing microbial communities with considerable differences to exhibit similar reactions under comparable salinities. Microbial metabolism enhances the chemical diversity of DOM in river−ocean continua, providing energy sources for microbial development, with salinity playing a regulatory role in this long-term equilibrium between microbes and DOM. The co-occurrence network analysis reveals the regulatory role of salinity in the promotion and inhibition of specific DOM transformation under the interactions of microbial cooperation and competition at the molecular level. This study provides molecular insights into the important roles of the salinity in manipulating microbial community the DOM transformation along the salinity gradient in river−ocean continua.

■ ASSOCIATED CONTENT

Supporting Information

The Supporting Information is available free of charge at https://pubs.acs.org/doi/10.1021/acsestwater.4c00832.

Details of procedures of FT-ICR MS analysis, 16S amplicon sequencing and bioinformatic processing, fluorescence components obtained using the EEM−PARAFAC model, Van Krevelen diagrams of the DOM formulas, heatmap of genus-level species composition for clustered organisms, GraPhlAn phylogenetic tree diagram, general water quality of surface water samples across the salinity gradient, description of absorption and fluorescence parameters, matching results of four fluorescent components identified by parallel factor analysis (PARAFAC), molecular characterization of DOM before and after biodegradation, potential biochemical transformations between DOM molecules in different salinity gradients, summary of the reactions considered in the linkage analysis, and molecular characters of common presence molecules (PDF)

■ AUTHOR INFORMATION

Corresponding Authors

Haijun He − *Guangzhou Marine Geological Survey, Guangzhou 511458, P.R. China*; Email: hehaijun1986@126.com

Mingzhi Huang − *Guangdong Provincial Engineering Research Center of Intelligent Low-carbon Pollution Prevention and Digital Technology & Guangdong Provincial Key Laboratory of Chemical Pollution and Environmental Safety & MOE Key Laboratory of Theoretical Chemistry of Environment, School of Environment, South China Normal University, Guangzhou 510006, P.R. China; SCNU (NAN'AN) Green and Low-carbon Innovation Center & Nan'an SCNU Institute of Green and Low-carbon Research, South China Normal University, Quanzhou 362300, P.R. China*; orcid.org/0000-0002-2592-3544; Email: mingzhi.huang@m.scnu.edu.cn

Authors

Chao Zhang − *Guangdong Provincial Engineering Research Center of Intelligent Low-carbon Pollution Prevention and Digital Technology & Guangdong Provincial Key Laboratory of Chemical Pollution and Environmental Safety & MOE Key Laboratory of Theoretical Chemistry of Environment, School of Environment, South China Normal University, Guangzhou 510006, P.R. China; SCNU (NAN'AN) Green and Low-carbon Innovation Center & Nan'an SCNU Institute of Green and Low-carbon Research, South China Normal University, Quanzhou 362300, P.R. China; Engler-Bunte-Institut, Water Chemistry and Water Technology, Karlsruhe Institute of Technology, Karlsruhe 76131, Germany*

Yingqiang Li − *Guangdong Provincial Engineering Research Center of Intelligent Low-carbon Pollution Prevention and Digital Technology & Guangdong Provincial Key Laboratory of Chemical Pollution and Environmental Safety & MOE Key Laboratory of Theoretical Chemistry of Environment, School of Environment, South China Normal University, Guangzhou 510006, P.R. China; SCNU (NAN'AN) Green and Low-carbon Innovation Center & Nan'an SCNU Institute of Green and Low-carbon Research, South China Normal University, Quanzhou 362300, P.R. China*

Junyu Zhu − *Guangdong Provincial Engineering Research Center of Intelligent Low-carbon Pollution Prevention and Digital Technology & Guangdong Provincial Key Laboratory of Chemical Pollution and Environmental Safety & MOE Key Laboratory of Theoretical Chemistry of Environment, School of Environment, South China Normal University, Guangzhou 510006, P.R. China; SCNU (NAN'AN) Green and Low-carbon Innovation Center & Nan'an SCNU Institute of Green and Low-carbon Research, South China Normal University, Quanzhou 362300, P.R. China*

Zhe Zhang − *Department of Chemical and Environmental Engineering (ChEE), University of Cincinnati, Cincinnati, Ohio 45221-0012, United States*; orcid.org/0000-0003-3249-0465

Yue Xie − *Guangdong Provincial Engineering Research Center of Intelligent Low-carbon Pollution Prevention and Digital Technology & Guangdong Provincial Key Laboratory of Chemical Pollution and Environmental Safety & MOE Key Laboratory of Theoretical Chemistry of Environment, School of Environment, South China Normal University, Guangzhou 510006, P.R. China; SCNU (NAN'AN) Green and Low-carbon Innovation Center & Nan'an SCNU Institute of Green and Low-carbon Research, South China Normal University, Quanzhou 362300, P.R. China*

Shuna Fu − *Agilent Technologies (China) Co. Ltd., Guangzhou 510005, P.R. China*

Wanbing Zheng − *Guangdong Provincial Engineering Research Center of Intelligent Low-carbon Pollution Prevention and Digital Technology & Guangdong Provincial*

https://doi.org/10.1021/acsestwater.4c00832
ACS EST Water 2025, 5, 2096−2109

Key Laboratory of Chemical Pollution and Environmental Safety & MOE Key Laboratory of Theoretical Chemistry of Environment, School of Environment, South China Normal University, Guangzhou 510006, P.R. China; SCNU (NAN'AN) Green and Low-carbon Innovation Center & Nan'an SCNU Institute of Green and Low-carbon Research, South China Normal University, Quanzhou 362300, P.R. China

Zihan Shen − *Guangdong Provincial Engineering Research Center of Intelligent Low-carbon Pollution Prevention and Digital Technology & Guangdong Provincial Key Laboratory of Chemical Pollution and Environmental Safety & MOE Key Laboratory of Theoretical Chemistry of Environment, School of Environment, South China Normal University, Guangzhou 510006, P.R. China; SCNU (NAN'AN) Green and Low-carbon Innovation Center & Nan'an SCNU Institute of Green and Low-carbon Research, South China Normal University, Quanzhou 362300, P.R. China*

Bangxing Ren − *Department of Chemical and Environmental Engineering (ChEE), University of Cincinnati, Cincinnati, Ohio 45221-0012, United States*

Zhenguo Chen − *Guangdong Provincial Engineering Research Center of Intelligent Low-carbon Pollution Prevention and Digital Technology & Guangdong Provincial Key Laboratory of Chemical Pollution and Environmental Safety & MOE Key Laboratory of Theoretical Chemistry of Environment, School of Environment, South China Normal University, Guangzhou 510006, P.R. China; SCNU (NAN'AN) Green and Low-carbon Innovation Center & Nan'an SCNU Institute of Green and Low-carbon Research, South China Normal University, Quanzhou 362300, P.R. China*

Guang-Guo Ying − *Guangdong Provincial Engineering Research Center of Intelligent Low-carbon Pollution Prevention and Digital Technology & Guangdong Provincial Key Laboratory of Chemical Pollution and Environmental Safety & MOE Key Laboratory of Theoretical Chemistry of Environment, School of Environment, South China Normal University, Guangzhou 510006, P.R. China;* orcid.org/0000-0002-3387-1078

Harald Horn − *Engler-Bunte-Institut, Water Chemistry and Water Technology, Karlsruhe Institute of Technology, Karlsruhe 76131, Germany*

Amy M. McKenna − *National High Magnetic Field Laboratory, Florida State University, Tallahassee, Florida 32306-4390, United States;* orcid.org/0000-0001-7213-521X

Complete contact information is available at: https://pubs.acs.org/10.1021/acsestwater.4c00832

Author Contributions

#C.Z., Y.L., and J.Z. contributed to the work equally and should be regarded as cofirst authors.

Author Contributions

C.Z., J.Z., and Y.L. contributed to the work equally and should be regarded as cofirst authors. C.Z. designed this study. C.Z. and Z.Z. wrote the original draft of this manuscript. Y.L., C.Z., Y.X., W.Z., and Z.S. performed the experiments and collected the data. J.Z., C.Z., S.F., B.R., and Z.C. contributed in the data analysis. H.H. (Haijun He) participated in the sample collection, sample detection, and data interpretation. A.M.M. and H.H. (Prof. Harald Horn) provided technical guidance in the areas of microbial DOM transformation and FT-ICR MS processing, respectively, and manuscript modification. M.H. and G.G.Y. supervised the analyses, including data interpretation and discussion.

Notes

The authors declare no competing financial interest.

■ ACKNOWLEDGMENTS

This work was supported by the National Natural Science Foundation of China (nos. 41977300 and 42277053), Science and Technology Program of Quanzhou (China) (no. 2022C003R), and Science and Technology Program of Qingyuan (China) (no. 2022KJJH020). The author C. Zhang acknowledges the support from Alexander von Humboldt Stiftung, National Natural Science Foundation of China (no. 42407308), China Postdoctoral Science Foundation (no. 2024M760988), and Young Teachers Research Cultivation Project of South China Normal University (no. 23KJ02). We are also deeply grateful for the data analysis supports provided by Agilent Technologies (China) Co. Ltd. (Guangzhou), and especially Ms. Shuna Fu.

■ REFERENCES

(1) Li, S. D.; Meng, L. Z.; Zhao, C.; Gu, Y.; Spencer, R. G. M.; Álvarez-Salgado, X. A.; Kellerman, A. M.; McKenna, A. M.; Huang, T.; Yang, H.; Huang, C. C. Spatiotemporal response of dissolved organic matter diversity to natural and anthropogenic forces along the whole mainstream of the Yangtze River. *Water Res.* **2023**, *234*, No. 119812.

(2) Zhang, C.; Dionysiou, D. D.; Wen, R. B.; Zhang, H. K.; Wan, X.; Wang, X. Z.; Li, F.; Li, Y. Q.; Zhou, Q.; Ying, G.-G.; Huang, M. Z. Inference of emission history of neonicotinoid pesticides from marine sediment cores impacted by riverine runoff of a developed agricultural region: The Pearl River Basin, China. *Water Res.* **2022**, *218*, No. 118475.

(3) Raymond, P. A.; Spencer, R. G. Riverine DOM, Biogeochemistry of Marine Dissolved Organic Matter. *Elsevier* **2015**, 509−533.

(4) Hansell, D. A.; Carlson, C. A. Net community production of dissolved organic carbon. *Global Biogeochem. Cycles* **1998**, *12*, 443−453.

(5) Hansell, D. A.; Carlson, C. A. *Biogeochemistry of Marine Dissolved Organic Matter*. Academic Press 2014.

(6) Li, Y. Y.; Zhou, Y. Q.; Zhou, L.; Zhang, Y. L.; Xu, H.; Jang, K. S.; Kothawala, D. N.; Spencer, R. G. M.; Jeppesen, E.; Brookes, J. D.; Davidson, T. A.; Wu, F. C. Changes in Water Chemistry Associated with Rainstorm Events Increase Carbon Emissions from the Inflowing River Mouth of a Major Drinking Water Reservoir. *Environ. Sci. Technol.* **2022**, *56* (22), 16494−16505.

(7) Zhou, Y. Q.; Yu, X. Q.; Zhou, L.; Zhang, Y. L.; Xu, H.; Zhu, M. Y.; Zhu, G. W.; Jang, K. S.; Spencer, R. G. M.; Jeppesen, E.; Brookes, J. D.; Kothawala, D. N.; Wu, F. C. Rainstorms drive export of aromatic and concurrent bio-labile organic matter to a large eutrophic lake and its major tributaries. *Water Res.* **2023**, *229*, No. 119448.

(8) Vaughn, D. R.; Kellerman, A. M.; Wickland, K. P.; Striegl, R. G.; Podgorski, D. C.; Hawkings, J. R.; Nienhuis, J. H.; Dornblaser, M. M.; Stets, E. G.; Spencer, R. G. M. Bioavailability of dissolved organic matter varies with anthropogenic landcover in the Upper Mississippi River Basin. *Water Res.* **2023**, *229*, No. 119357.

(9) Yu, S. Y.; Lv, J. T.; Jiang, L.; Geng, P. Y.; Cao, D.; Wang, Y. W. Changes of Soil Dissolved Organic Matter and Its Relationship with Microbial Community along the Hailuogou Glacier Forefield Chronosequence. *Environ. Sci. Technol.* **2023**, *57* (9), 4027−4038.

(10) Ma, T.; Zhu, S.; Wang, Z.; Chen, D.; Dai, G.; Feng, B.; Su, X.; Hu, H.; Li, K.; Han, W.; Liang, C.; Bai, Y.; Feng, X. Divergent accumulation of microbial necromass and plant lignin components in grassland soils. *Nat. Commun.* **2018**, *9*, 3480−3488.

(11) Kallenbach, C. M.; Frey, S. D.; Grandy, A. S. Direct evidence for microbial-derived soil organic matter formation and its ecophysiological controls. *Nat. Commun.* **2016**, *7*, 13630−13639.
(12) Kellerman, A. M.; Guillemette, F.; Podgorski, D. C.; Aiken, G. R.; Butler, K. D.; Spencer, R. G. M. Unifying concepts linking dissolved organic matter composition to persistence in aquatic ecosystems. *Environ. Sci. Technol.* **2018**, *52*, 2538−2548.
(13) Zhang, C.; Yi, X. Y.; Chen, C.; Tian, D.; Liu, H. B.; Xie, L. T.; Zhu, X. P.; Huang, M. Z.; Ying, G.-G. Contamination of neonicotinoid insecticides in soil-water-sediment systems of the urban and rural areas in a rapidly developing region: Guangzhou, South China. *Environ. Int.* **2020**, *139*, No. 105719.
(14) Yi, X. H.; Zhang, C.; Liu, H. B.; Wu, R. R.; Tian, D.; Ruan, J. J.; Zhang, T.; Huang, M. Z.; Ying, G. G. Occurrence and distribution of neonicotinoid insecticides in surface water and sediment of the Guangzhou section of the Pearl River, South China. *Environ. Pollut.* **2019**, *251*, 892−900.
(15) Zhang, C.; Tian, D.; Yi, X. H.; Zhang, T.; Ruan, J. J.; Wu, R. R.; Chen, C.; Huang, M. Z.; Ying, G. G. Occurrence, distribution and seasonal variation of five neonicotinoid insecticides in surface water and sediment of the Pearl Rivers, South China. *Chemosphere* **2019**, *217*, 437−446.
(16) Liang, C.; Schimel, J. P.; Jastrow, J. D. The importance of anabolism in microbial control over soil carbon storage. *Nat. Microbiol.* **2017**, *2*, 17105−17110.
(17) Ng, E. L.; Patti, A. F.; Rose, M. T.; Schefe, C. R.; Wilkinson, K.; Smernik, R. J.; Cavagnaro, T. R. Does the chemical nature of soil carbon drive the structure and functioning of soil microbial communities? *Soil Biol. Biochem.* **2014**, *70*, 54−61.
(18) Holmes, D. E.; Dang, Y.; Walker, D. J. F.; Lovley, D. R. The electrically conductive pili of Geobacter species are a recently evolved feature for extracellular electron transfer. *Microb. Genomics* **2016**, *2*, No. e000072.
(19) Shu, W. S.; Huang, L. N. Microbial diversity in extreme environments. *Nat. Rev. Microbiol.* **2022**, *20*, 219−235.
(20) Yang, J.; Jiang, H.; Liu, W.; Huang, L. Q.; Huang, J. R.; Wang, B. C.; Dong, H. L.; Chu, R. K.; Tolic, N. Potential utilization of terrestrially derived dissolved organic matter by aquatic microbial communities in saline lakes. *ISME J.* **2020**, *14*, 2313−2324.
(21) Bouvier, T. C.; del Giorgio, P. A. Compositional changes in free-living bacterial communities along a salinity gradient in two temperate estuaries. *Limnol. Oceanogr.* **2002**, *47* (2), 453−470.
(22) Harrison, P. J.; Yin, K. D.; Lee, J. H. W.; Gan, J. P.; Liu, H. B. Physical−biological coupling in the Pearl River Estuary. *Cont. Shelf Res.* **2008**, *28* (12), 1405−1415.
(23) Stedmon, C. A.; Granskog, M.; Dodd, P. A. An approach to estimate the freshwater contribution from glacial melt and precipitation in East Greenland shelf waters using colored dissolved organic matter (CDOM). *Journal of Geophysical Research: Oceans* **2015**, *120*, 1107−1117.
(24) Weishaar, J. L.; Aiken, G. R.; Bergamaschi, B. A.; Fram, M. S.; Fujii, R.; Mopper, K. Evaluation of specific ultravoilet absorbance as an indicator of the chemical composition of reactivity of dissolved organic matter. *Environ. Sci. Technol.* **2003**, *37*, 4702−4708.
(25) Helms, J. R.; Stubbins, A.; Ritchie, J. D.; Minor, E. C.; Kieber, D. J.; Mopper, K. Absorption spectral slopes and slope ratios as indicators of molecular weight, source, and photobleaching of chromophoric dissolved organic matter. *Limnology and Oceanography* **2008**, *53* (3), 955−969.
(26) Zhang, B.; Shan, C.; Wang, S.; Fang, Z.; Pan, B. Unveiling the transformation of dissolved organic matter during ozonation of municipal secondary effluent based on FT-ICR-MS and spectral analysis. *Water Res.* **2021**, *188*, No. 116484.
(27) Kellerman, A. M.; Dittmar, T.; Kothawala, D. N.; Tranvik, L. J. Chemodiversity of dissolved organic matter in lakes driven by climate and hydrology. *Nat. Commun.* **2014**, *5* (1), 1−8.
(28) Zhang, J.; McKenna, A. M.; Zhu, M. Macromolecular characterization of compound selectivity for oxidation and oxidative alterations of dissolved organic matter by manganese oxide. *Environ. Sci. Technol.* **2021**, *55* (11), 7741−7751.
(29) Yadav, S.; Chattopadhyay, D. Lignin: the Building Block of Defense Responses to Stress in Plants. *J. Plant Growth Regul.* **2023**, *42*, 6652−6666.
(30) Lu, F.; Wang, C.; Chen, M.; Yue, F.; Ralph, J. A facile spectroscopic method for measuring lignin content in lignocellulosic biomass. *Green Chem.* **2021**, *23*, 5106−5112.
(31) Chen, Z.; Doering, P. H.; Ashton, M.; et al. Mixing Behavior of Colored Dissolved Organic Matter and Its Potential Ecological Implication in the Caloosahatchee River Estuary, Florida. *Estuaries and Coasts* **2015**, *38*, 1706−1718.
(32) McKnight, D. M.; Elizabeth, B. W.; Paul, W. K.; et al. Spectrofluorometric characterization of dissolved organic matter for indication of precursor organic material and aromaticity. *Limnol. Oceanogr.* **2001**, *46*, 38.
(33) Huguet, A.; Vacher, L.; Relexans, S.; et al. Properties of fluorescent dissolved organic matter in the Gironde Estuary. *Org. Geochem.* **2009**, *40* (6), 706−719.
(34) Wickland, K. P.; Neff, J. C.; Aiken, G. R. Dissolved organic carbon in Alaskan boreal forest: sources, chemical characteristics, and biodegradability. *Ecosystems* **2007**, *10* (8), 1323−1340.
(35) Li, R. F.; Zhang, J.; Krebs, P. Consumption- and Income-Based Sectoral Emissions of Polycyclic Aromatic Hydrocarbons in China from 2002 to 2017. *Environ. Sci. Technol.* **2021**, *55* (6), 3582−3592.
(36) Hou, C. Y.; Chen, L.; Dong, Y. W.; Yang, Y. L.; Zhang, X. H. Unraveling dissolved organic matter in drinking water through integrated ozonation/ceramic membrane and biological activated carbon process using FT-ICR MS. *Water Res.* **2022**, *222*, No. 118881.
(37) Yuan, Z.; He, C.; Shi, Q.; Xu, C.; Li, Z.; Wang, C.; Zhao, H.; Ni, J. Molecular insights into the transformation of dissolved organic matter in landfill leachate concentrate during biodegradation and coagulation processes using ESI FT-ICR MS. *Environ. Sci. Technol.* **2017**, *51* (14), 8110−8118.
(38) Tan, C.; Chen, S. Y.; Zhang, H. Y.; Ma, Y.; Qu, Z. Y.; Yan, N.; Zhang, Y. M.; Rittmann, B. E. The Roles of *Rhodococcus Ruber* in Denitrification with Quinoline as the Electron Donor. *Sci. Total Environ.* **2023**, *902*, No. 166128.
(39) Liu, X.; Xin, X.; Yang, W.; et al. Effect mechanism of micron-scale zero-valent iron enhanced pyrite-driven denitrification biofilter for nitrogen and phosphorus removal. *Bioprocess Biosyst. Eng.* **2023**, *46*, 1847−1860.
(40) Arat, S.; Bullerjahn, G. S.; Laubenbacher, R. A Network Biology Approach to Denitrification in Pseudomonas aeruginosa. *PLoS One* **2015**, *10* (2), No. e0118235.
(41) Props, R.; Denef, V. J.; Nojiri, H. Temperature and Nutrient Levels Correspond with Lineage-Specific Microdiversification in the Ubiquitous and Abundant Freshwater Genus Limnohabitans. *Appl. Environ. Microbiol.* **2020**, *86*, No. e00140-20.
(42) Patureau, D.; Davison, J.; Bernet, N.; Moletta, R. Denitrification under various aeration conditions in Comamonas sp., strain SGLY2. *FEMS Microbiology Ecology* **1994**, *14* (1), 71−78.
(43) Ludden, P. W.; Roberts, G. P. Nitrogen fixation by photosynthetic bacteria. *Photosynthesis Research* **2002**, *73*, 115−118.
(44) Komova, A. V.; Bakhmutova, E. D.; Izotova, A. O.; et al. Nitrogen Fixation Activity and Genome Analysis of a Moderately Haloalkaliphilic Anoxygenic Phototrophic Bacterium Rhodovulum tesquicola. *Microorganisms* **2022**, *10*, 1615.
(45) Masepohl, B.; Drepper, T.; Klipp, W. Nitrogen Fixation in the Photosynthetic Purple Bacterium Rhodobacter capsulatus. In: Klipp, W.; Masepohl, B.; Gallon, J. R.; Newton, W. E. (eds) *Genetics and Regulation of Nitrogen Fixation in Free-Living Bacteria*. Nitrogen Fixation: Origins, Applications, and Research Progress; Springer: Dordrecht 2004, vol 2.
(46) Wang, L.; Lin, Y.; Ye, L.; Qian, Y.; Shi, Y.; Xu, K.; Ren, H.; Geng, J. Microbial Roles in Dissolved Organic Matter Transformation in Full-Scale Wastewater Treatment Processes Revealed by Reactomics and Comparative Genomics. *Environ. Sci. Technol.* **2021**, *55* (16), 11294−11307.

https://doi.org/10.1021/acsestwater.4c00832
ACS EST Water 2025, 5, 2096−2109

(47) Horemans, B.; Vandermaesen, J.; Smolders, E.; Springael, D. Cooperative dissolved organic carbon assimilation by a linuron-degrading bacterial consortium. *FEMS Microbiol. Ecol.* **2013**, *84*, 35−46.
(48) Zhou, S. F.; Liao, Z. Y.; Zhang, B. P.; Hou, R.; Wang, Y.; Zhou, S. G.; Zhang, Y. F.; Ren, Z. J.; Yuan, Y. Photochemical Behavior of Microbial Extracellular Polymeric Substances in the Aquatic Environment. *Environ. Sci. Technol.* **2021**, *55* (22), 15090−15099.
(49) Xiao, K. K.; Abbt-Braun, G.; Horn, H. Changes in the characteristics of dissolved organic matter during sludge treatment: A critical review. *Water Res.* **2020**, *187*, No. 116441.

https://doi.org/10.1021/acsestwater.4c00832
ACS EST Water 2025, 5, 2096−2109